

Three-loop jet function for boosted top quarks

Vicent Mateu,^{a,*} Alberto M. Clavero^a and Maximilian Stahlhofen^b

^a*Departamento de Física Fundamental e IUFFyM,
Universidad de Salamanca, E-37008 Salamanca, Spain*

^b*Albert-Ludwigs-Universität Freiburg, Physikalisches Institut,
D-79104 Freiburg, Germany*

*E-mail: vmateu@usal.es, albertomarcla@usal.es,
maximilian.stahlhofen@physik.uni-freiburg.de*

We present the calculation of the inclusive jet function for highly energetic heavy quarks at order $O(\alpha_s^3)$ using boosted Heavy-Quark Effective Theory (bHQET). This jet function describes the effect of collinear radiation emitted by energetic heavy quarks on observables dependent on the jet invariant mass M . In particular, we focus on the regime $M^2 - m^2 \ll m^2$, which is relevant for boosted top quark production at high-energy colliders in the resonance region. Our results are consistent with non-Abelian exponentiation and reproduce the known cusp and non-cusp anomalous dimensions up to three loops. We also verify that the $n_\ell^2 \alpha_s^3$ contribution, with n_ℓ denoting the number of light quark flavors, agrees with predictions from renormalon calculus. This calculation completes the list of ingredients required for the N^3LL' resummed (self-normalized) thrust distribution, an essential component for calibrating the top quark mass parameter in parton-shower Monte Carlo generators. It likewise contributes to the invariant-mass distribution of reconstructed top quarks, enabling precise mass determinations at future lepton colliders. Finally, we determine the relation between the pole and two short-distance jet-mass schemes at $O(\alpha_s^3)$ and provide an estimate of the non-logarithmic part of the four-loop jet function based on renormalon dominance.

*The European Physical Society Conference on High Energy Physics (EPS-HEP2025)
7-11 July 2025
Marseille, France*

*Speaker

1. Introduction

Precise determinations of the top quark mass play a central role in testing the Standard Model (SM). Its value critically impacts the electroweak vacuum stability and affects other SM parameters such as the W - and Higgs-boson masses. Obtaining a precise measurement of the top mass m is therefore essential for performing consistency checks of the SM.

Since the top quark decays before it can hadronize, many analyses attempt to determine its mass using kinematic information from its decay products. These direct experimental measurements have reached a precision of approximately 300 MeV at the Tevatron and LHC, and prospects indicate that this uncertainty can be further reduced. The mass determined by direct measurements does not, however, correspond to any well-defined mass within quantum field theory, but rather to a mass parameter inherent to parton-shower Monte Carlo (MC) generators, dubbed m^{MC} .

Event shapes at e^+e^- colliders have been extensively used to probe the QCD structure, tune MC generators, and determine the strong coupling α_s with high precision. For processes involving boosted top quark pairs, it has been shown that the top mass can be determined (in a suitable short-distance scheme) with uncertainty smaller than Λ_{QCD} using event shapes related to hemisphere invariant masses [1, 2]. The maximal sensitivity to the top mass occurs in the peak region of the hemisphere mass distribution, characterized by $M^2 - m^2 \equiv m\hat{s}$ where $m \gg \hat{s} \sim \Gamma_t \gg \Lambda_{\text{QCD}}$. In this region, highly energetic top quarks can be described using boosted Heavy Quark Effective Theory (bHQET) matched to Soft Collinear Effective Theory (SCET). This EFT framework enables the resummation of large logarithms, consistently includes the top decay width Γ_t and accounts for soft hadronization power corrections from first principles.

At leading power in the expansion in powers of m/Q , Γ_t/m , and \hat{s}/m (with Q the center-of-mass energy), the dijet factorization theorem for the double hemisphere invariant mass differential distribution reads [1]

$$\begin{aligned} \frac{d^2\sigma^{(\text{dijet})}}{dM_1^2 dM_2^2} &= \sigma_0 H_Q^{(n_\ell+1)}(Q, \mu) H_m\left(m, \frac{Q}{m}, \mu\right) \int d\ell^+ d\ell^- S^{(n_\ell)}(\ell^+, \ell^-, \mu) \\ &\times B_n^{(n_\ell)}\left(\frac{M_1^2 - Q\ell^+}{m} - m, \Gamma_t, \mu\right) B_{\bar{n}}^{(n_\ell)}\left(\frac{M_2^2 - Q\ell^-}{m} - m, \Gamma_t, \mu\right). \end{aligned} \quad (1)$$

This formula contains the massless hard H_Q and soft functions S coming from the corresponding SCET factorization theorem, which are known at three and two loops, respectively. The matching factor H_m encodes the effect of soft and collinear mass-modes, and its rapidity-resummed expression is currently known at NNLL' (N³LO) [3]. The bHQET jet functions B_n and $B_{\bar{n}}$, identical due to charge conjugation, describe the dynamics of the back-to-back boosted heavy-quark jets. The main aim of our work is to extend the calculation of the jet function B_n , previously determined up to two-loop order [4], to three loops. Details of this calculation have been published in Ref. [5].

Our result can be used to obtain the di-hemisphere mass, thrust, heavy jet mass and C-parameter cross sections in the peak region at N³LL'. In addition, it is the last missing piece to achieve an N³LL'-precise calibration between m^{MC} and the MSR mass m^{MSR} [6]. Finally, it will eventually improve the precision of (indirect) top mass determinations from boosted-top production at a future lepton collider [7, 8].

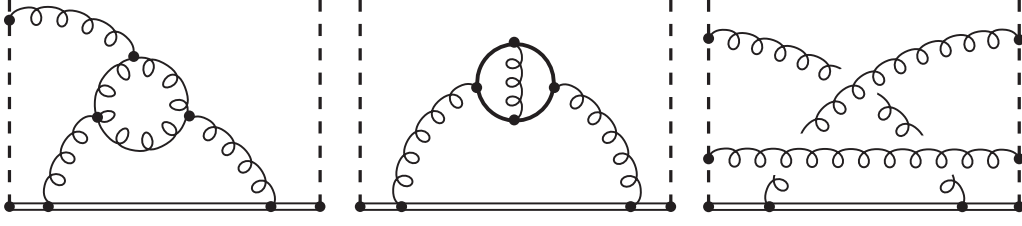


Figure 1: Sample of Feynman diagrams contributing to the jet function at three loops. Double, curly, dashed and solid lines represent heavy-quarks, gluons, light-like Wilson lines and light quarks, respectively.

2. Theoretical setup

The bHQET jet function for stable top quarks with heavy-quark mass expressed in the pole scheme is defined through the forward-scattering matrix element [1, 4]

$$\mathcal{B}^{\text{bare}}(\hat{s}) \equiv \frac{-i}{4\pi N_c m} \int d^d z e^{ir \cdot z} \langle 0 | T \{ \bar{h}_v(0) W_n(0) W_n^\dagger(z) h_v(z) \} | 0 \rangle = -\frac{1}{\pi m \hat{s}} + \mathcal{O}(\alpha_s), \quad (2)$$

where h_v is the bHQET heavy-quark field with velocity v^μ , such that $\hat{s} = 2v \cdot r$ and $v^2 = 1$. W_n is the n -collinear Wilson line, with $n^\mu = (1, \vec{n})$ a light-like vector ($|\vec{n}| = 1$) and \vec{n} collinear to the jet direction. Finally, N_c denotes the number of colors. The renormalized bHQET jet function $B \equiv B_n$ is obtained through the imaginary part of the matrix element in Eq. (2),

$$B(\hat{s}) \equiv \text{Im}[\mathcal{B}(\hat{s} + i\eta)] = \frac{1}{m} \delta(\hat{s}) + \mathcal{O}(\alpha_s), \quad (3)$$

where η is a positive infinitesimal. The expression for unstable quarks is obtained by shifting $\eta \rightarrow \Gamma_t$ in Eq. (3). In order to efficiently solve the jet function's renormalization group equation (RGE), it is convenient to work with the Fourier transform of B , also referred to as the position-space jet function, and its exponentiated form

$$\tilde{B}(x) \equiv \int d\hat{s} e^{-i(x-i\eta)\hat{s}} B(\hat{s}), \quad \tilde{B}(x) = \frac{1}{m} \exp[\tilde{b}(x)]. \quad (4)$$

As argued in Ref. [4], the jet function is subject to non-Abelian exponentiation, which means that the exponent $\tilde{b}(x)$ exclusively contains fully connected color factors [9]. This class of color factors corresponds to that of Feynman diagrams that remain connected once all Wilson lines are removed from the graph. In particular, this implies that, at $\mathcal{O}(\alpha_s^3)$, the color structures $C_F^2 C_A$ and C_F^3 must be absent and only diagrams involving a fermion loop with four gluon attachments, like the second diagram in Fig. 1, can contribute to the $C_F^2 T_F n_\ell$ term of $\tilde{b}(x)$.

To regulate UV and IR divergences in loop diagrams, we employ dimensional regularization with $d = 4 - 2\epsilon$. For the renormalization of the jet function and the strong coupling we employ the $\overline{\text{MS}}$ scheme, while the heavy-quark mass m is defined (for the time being) in the pole scheme. The divergences in the momentum-space bare jet function are removed by convolving it with a renormalization factor $Z_B(\hat{s}, \mu)$ which depends on the $\overline{\text{MS}}$ renormalization scale μ .

	1 loop	2 loops	3 loops
Feynman diagrams	4	~50	~1100
Scalar integrals	3	~70	~5400
Master integrals	1	3	20

Table 1: Number of Feynman diagrams, non-vanishing scalar integrals, and master integrals contributing to the jet function at one, two and three loops. Numbers may vary depending on the particular setup, and should be understood as just a rough complexity measure.

Hence, the renormalized jet function is μ -dependent and satisfies a RGE, which in position space reads

$$\frac{d \log [m \tilde{B}(x, \mu)]}{d \log \mu} = 2\Gamma^c[\alpha_s(\mu)] \log(i e^{\gamma_E} x \mu) + \gamma_B^{\text{nc}}[\alpha_s(\mu)]. \quad (5)$$

Γ^c and γ_B^{nc} are the cusp and non-cusp anomalous dimensions, respectively. The solution of the RGE in momentum space enables resummation of large logarithms of the type $\log(\hat{s}/m)$ through scale evolution. In our paper [5] we provide relations among the coefficients appearing in the perturbative expansion of the various versions of the jet function, like the ones in Eqs. (2), (3) and (4). From the RGE, we also derive relations that express the logarithmic coefficients appearing in the renormalized jet function in terms of the cusp, non-cusp and strong-coupling anomalous dimensions and lower-loop non-logarithmic coefficients. These relations enable efficient code implementation of the RGE and conversion between jet function variants.

The jet function as defined in Eq. (3) exhibits an infrared renormalon ambiguity. The renormalon leads to an asymptotically divergent behavior of the perturbative series in α_s unless it is canceled by switching to a low-scale short-distance scheme such as the MSR mass. The corresponding scheme change is implemented by shifting the argument of the jet function,

$$B(\hat{s}, \delta m, \Gamma_t, \mu) = \text{Im}[\mathcal{B}(\hat{s} - 2\delta m + i\Gamma_t, \mu)] = \exp\left(-2\delta m \frac{\partial}{\partial \hat{s}}\right) B(\hat{s}, 0, \Gamma_t, \mu), \quad (6)$$

where $\delta m = m - m_{\text{SD}}$ defines the short-distance mass m_{SD} . We study two alternative jet-mass schemes: the *derivative scheme* [4] and the *non-derivative scheme* [10], defined respectively through

$$\begin{aligned} \delta m^J(\mu, R) &= \frac{Re^{\gamma_E}}{2} \left\{ \frac{d}{d \log(ix)} \log[m \tilde{B}(x, \mu)] \right\}_{ixe^{\gamma_E}=1/R}, \\ \delta m^{J'}(R) &= \frac{Re^{\gamma_E}}{2} \log\left[m \tilde{B}\left(\frac{1}{iRe^{\gamma_E}}, R\right)\right]. \end{aligned} \quad (7)$$

Both schemes remove the renormalon and exhibit different perturbative behavior, which we compare to the MSR mass as a benchmark. Since $\delta m^{J'}$ does not involve any derivatives, the asymptotic behavior sets in faster than for the original jet-mass scheme, which may be advantageous in situations where only few perturbative orders are known. On the other hand, the derivative jet-mass scheme requires less perturbative ingredients at a given finite order than the non-derivative scheme [5].

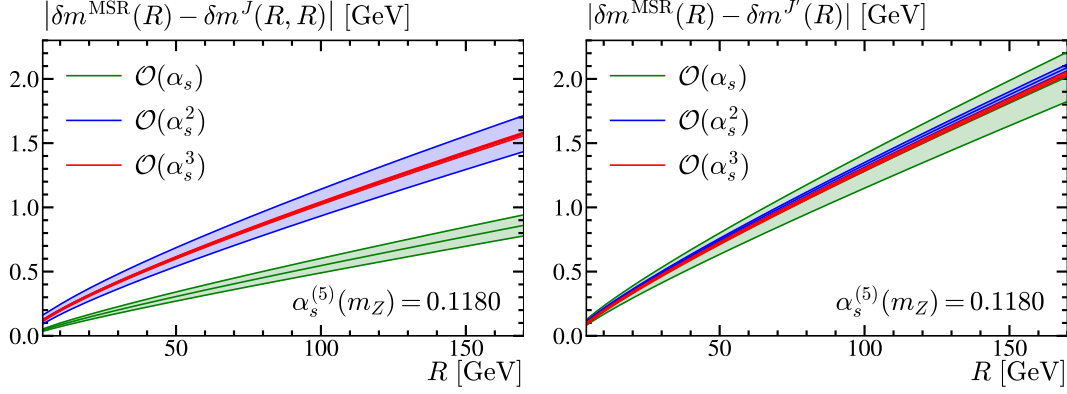


Figure 2: Difference between the heavy quark MSR and jet masses in the derivative (left) and non-derivative (right) schemes in absolute value. In the plots we use $n_\ell = 5$ for the number of active light flavors and $\alpha_s^{(n_\ell=5)}(m_Z) = 0.1180$. For both masses we expand $\alpha_s(R)$ in terms of $\alpha_s(\mu)$, and generate uncertainty bands varying μ in the range $R/2$ to $2R$.

3. Computation of the jet function

Our computation of the bare jet function matrix element in Eq. (2), which in many aspects resembles that of the soft function for heavy-to-light quark decays [11], proceeds as follows:

1. Generation of Feynman diagrams contributing to the matrix element using `qgraf` [12].
2. Mapping of the diagrams to integral families based on the denominator structure. For this procedure we use the algorithm outlined in Ref. [13] implemented in `Looping` [14].
3. Reduction to scalar integrals using `FORM` [15] and the `color.h` package [16]. Linear dependencies between denominators are removed by applying the multivariate partial fractioning algorithm of Ref. [13]. Scaleless integrals are discarded and symmetries related to momentum shifts are exploited to reduce the number of occurring integrals. All these operations are automated by the `Looping` interface.
4. IBP reduction, using `FIRE` [17] and `LiteRed` [18], to express all scalar integrals in terms of a basis of master integrals (MIs). Additional relations between MIs are found through dimensional recurrence relations following [19].
5. Analytical calculation of the MIs. We employed the method described in Ref. [20], which relies on a basis of (quasi-)finite integrals that can be evaluated with `HyperInt` [21], and Mellin-Barnes techniques.
6. All diagrams are added up and the results for the MIs are inserted to obtain the bare jet function matrix element $\mathcal{B}^{\text{bare}}(\hat{s})$. Taking the imaginary part yields the bare jet function.

To illustrate the variety of three-loop Feynman diagrams involved in the computation, we show a selection of them in Fig. 1. The number of Feynman diagrams, non-vanishing scalar integrals, and MIs relevant for our jet function calculation at one, two, and three loops (which serves as a rough complexity measure) is displayed in Table 1.

4. Main results

Our main result is the non-logarithmic term of the exponent of the renormalized position-space bHQET jet function

$$\tilde{b}(x) = \sum_{l=1}^{\infty} \left(\frac{\alpha_s}{4\pi} \right)^l \sum_{k=0}^{l+1} \tilde{b}_{lk} \log^k(i e^{\gamma_E} x \mu). \quad (8)$$

at three loops (for $N_c = 3$),

$$\begin{aligned} \tilde{b}_{30} = & \left(\frac{203\pi^2\zeta_3}{27} - \frac{105398\zeta_3}{243} + \frac{236\zeta_3^2}{9} + \frac{902\zeta_5}{9} + \frac{31952191}{26244} + \frac{93821\pi^2}{8748} \right. \\ & \left. - \frac{3023\pi^4}{4860} + \frac{1031\pi^6}{10206} \right) C_F C_A^2 + \left(\frac{3488\zeta_3}{243} + \frac{846784}{6561} - \frac{8\pi^2}{243} + \frac{52\pi^4}{1215} \right) C_F T_F^2 n_\ell^2 \\ & + \left(\frac{10760\zeta_3}{81} + \frac{8\pi^2\zeta_3}{9} + \frac{224\zeta_5}{9} - \frac{124717}{486} - \frac{55\pi^2}{54} + \frac{148\pi^4}{405} \right) C_F^2 T_F n_\ell \\ & + \left(\frac{1664\zeta_3}{81} - \frac{76\pi^2\zeta_3}{27} - \frac{88\zeta_5}{3} - \frac{5273287}{6561} - \frac{12793\pi^2}{2187} - \frac{421\pi^4}{1215} \right) C_F C_A T_F n_\ell \\ & = 50.054n_\ell^2 - 1899.8n_\ell + 12834, \end{aligned} \quad (9)$$

where \tilde{b}_{30} is defined through the expansion series of the exponent of the position-space jet function in Eq. (8). The logarithmic terms of the exponent can be derived from the known anomalous dimensions and beta function coefficients in the $\alpha_s/(4\pi)$ expansion,

$$\tilde{b}_{l1} = \gamma_{l-1}^B + 2 \sum_{j=1}^{l-1} j \beta_{l-j-1} \tilde{b}_{j0}, \quad \tilde{b}_{l2} = \Gamma_{l-1}^c + \sum_{j=1}^{l-1} j \beta_{l-j-1} \tilde{b}_{j1}, \quad \tilde{b}_{lk} = \frac{2}{k} \sum_{j=k-2}^{l-1} j \beta_{l-j-1} \tilde{b}_{j,k-1}. \quad (10)$$

We also recomputed the one- and two-loop bare matrix element for arbitrary dimension d . Results can be found in our paper [5]. We validated our results through multiple stringent checks. We have performed the computation of the bare matrix element in a general covariant gauge and checked that the dependence on the gauge parameter drops out once expressed in terms of MIs. Our expression for the logarithm of the position-space jet function in Eq. (9) is consistent with non-Abelian exponentiation. Furthermore, we have checked that $\mathcal{B}^{\text{bare}}$ is free of C_F^3 and $C_F^2 C_A$, and only diagrams involving a fermion loop with four gluon attachments can contribute to the $C_F^2 T_F n_\ell$ term already before the $\varepsilon = (4-d)/2$ expansion. We also verified that the $C_F T_F^2 n_\ell^2$ term in Eq. (9) agrees with the prediction from renormalon calculus in Ref. [10], and our full computation reproduces the known three-loop anomalous dimension coefficients γ_2^B and Γ_2^c [11, 22–25]. Additionally, all MIs were checked numerically using pySecDec [26] and FIESTA [27] to $\mathcal{O}(\varepsilon^3)$.

4.1 Jet-Mass schemes and four-loop jet function estimate

Using our three-loop result, we obtain the relation between the pole and jet-mass schemes defined in Eq. (7) at $\mathcal{O}(\alpha_s^3)$. The explicit expressions are lengthy and provided in our paper. Figure. 2 compares the two jet-mass schemes to the MSR mass benchmark. Our analysis shows that the non-derivative scheme exhibits faster convergence, with the one-loop result already falling

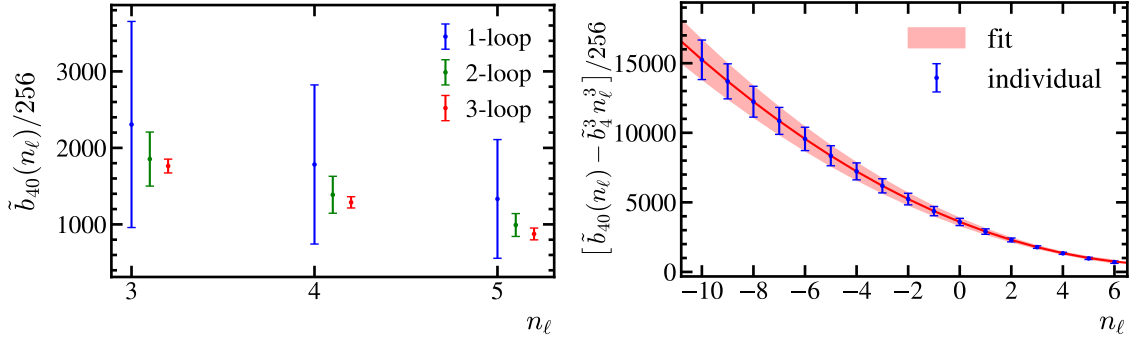


Figure 3: Estimates of \tilde{b}_{40} for various numbers of light flavors n_ℓ with $N_c = 3$. In the left panel, we show the estimates when including lower-order information up to one (blue), two (green), and three (red) loops. In the right panel, we use three-loop input to make predictions for a large set of n_ℓ values (in blue), and show as a red band the predictions obtained using the results for the various flavor coefficients. For details in the uncertainty calculation, we refer to our paper Ref. [5].

within the two- and three-loop uncertainty bands. The derivative scheme requires at least two loops for reliable results. Both schemes effectively remove the pole-mass renormalon at higher orders.

Based on renormalon dominance, we estimate the four-loop non-logarithmic coefficient using the R-evolution formalism applied to the non-derivative jet-mass scheme. We refer to [10] for details of the procedure. Specifically, we predict $\tilde{b}_{40}(n_\ell) = \sum_{i=0}^3 \tilde{b}_4^i n_\ell^i$, the non-logarithmic four-loop coefficient of the position-space jet function's exponent for different numbers of light flavors n_ℓ .

Our results are shown in Fig. 3. In the left panel, we present estimates of \tilde{b}_{40} for various n_ℓ values, utilizing lower-order information up to one (blue), two (green), and three (red) loops. In the right panel, we use three-loop input to make predictions for a wide range of n_ℓ values (in blue). The red band represents predictions obtained using the results for the various flavor coefficients, along with the corresponding uncertainties generated through error propagation. Our findings indicate that incorporating higher-order information leads to more precise estimates of \tilde{b}_{40} .

5. Conclusions

We have computed the inclusive bHQET jet function for boosted heavy quarks to three-loop accuracy, providing a universal ingredient in peak-region factorization theorems for event shape observables probing the top mass. Our result represents the last missing piece for $N^3\text{LL}'$ resummed predictions of the self-normalized thrust distributions used in Monte Carlo top mass calibration. We have also derived universal relations between different representations of the jet function and compared suitable short-distance mass schemes.

Future directions include computing the four-loop non-cusp anomalous dimension to achieve $N^4\text{LL}$ accuracy on the self-normalized thrust prediction, including effects of massive bottom quarks in the loop corrections, computing the missing three-loop contributions to H_m for full $N^3\text{LL}'$ predictions, and updating the calibration of the Monte-Carlo top mass to $N^3\text{LL}'$ accuracy using our new result [7, 8].

Acknowledgments

This work was supported in part by the Spanish MICIU/AEI/10.13039/501100011033 grant No. PID2022-141910NB-I00 and the JCyL grant SA091P24 under program EDU/841/2024. A. M. C. is supported by a FPU scholarship funded by the Spanish MICIU under grant no. FPU22/02506.

References

- [1] S. Fleming, A. H. Hoang, S. Mantry and I. W. Stewart, *Jets from massive unstable particles: Top-mass determination*, *Phys. Rev. D* **77** (2008) 074010, [[hep-ph/0703207](#)].
- [2] S. Fleming, A. H. Hoang, S. Mantry and I. W. Stewart, *Top Jets in the Peak Region: Factorization Analysis with NLL Resummation*, *Phys. Rev. D* **77** (2008) 114003, [[0711.2079](#)].
- [3] M. Fael, F. Lange, K. Schönwald and M. Steinhauser, *Singlet and nonsinglet three-loop massive form factors*, *Phys. Rev. D* **106** (2022) 034029, [[2207.00027](#)].
- [4] A. Jain, I. Scimemi and I. W. Stewart, *Two-loop Jet-Function and Jet-Mass for Top Quarks*, *Phys. Rev. D* **77** (2008) 094008, [[0801.0743](#)].
- [5] A. M. Clavero, R. Brüser, V. Mateu and M. Stahlhofen, *Three-loop jet function for boosted heavy quarks*, *JHEP* **04** (2025) 040, [[2412.06881](#)].
- [6] A. H. Hoang, A. Jain, C. Lepenik, V. Mateu, M. Preisser, I. Scimemi et al., *The MSR mass and the $O(\Lambda_{\text{QCD}})$ renormalon sum rule*, *JHEP* **04** (2018) 003, [[1704.01580](#)].
- [7] M. Butenschoen, B. Dehnadi, A. H. Hoang, V. Mateu, M. Preisser and I. W. Stewart, *Top Quark Mass Calibration for Monte Carlo Event Generators*, *Phys. Rev. Lett.* **117** (2016) 232001, [[1608.01318](#)].
- [8] B. Dehnadi, A. H. Hoang, O. L. Jin and V. Mateu, *Top quark mass calibration for Monte Carlo event generators — an update*, *JHEP* **12** (2023) 065, [[2309.00547](#)].
- [9] E. Gardi, J. M. Smillie and C. D. White, *The Non-Abelian Exponentiation theorem for multiple Wilson lines*, *JHEP* **06** (2013) 088, [[1304.7040](#)].
- [10] N. G. Gracia and V. Mateu, *Toward massless and massive event shapes in the large- β_0 limit*, *JHEP* **07** (2021) 229, [[2104.13942](#)].
- [11] R. Brüser, Z. L. Liu and M. Stahlhofen, *Three-loop soft function for heavy-to-light quark decays*, *JHEP* **03** (2020) 071, [[1911.04494](#)].
- [12] P. Nogueira, *Automatic Feynman Graph Generation*, *J. Comput. Phys.* **105** (1993) 279–289.
- [13] A. Pak, *The Toolbox of modern multi-loop calculations: novel analytic and semi-analytic techniques*, *J. Phys. Conf. Ser.* **368** (2012) 012049, [[1111.0868](#)].
- [14] R. Brüser, *Looping*, unpublished.

- [15] B. Ruijl, T. Ueda and J. Vermaseren, *FORM version 4.2*, [1707.06453](#).
- [16] T. van Ritbergen, A. N. Schellekens and J. A. M. Vermaseren, *Group theory factors for Feynman diagrams*, *Int. J. Mod. Phys. A* **14** (1999) 41–96, [[hep-ph/9802376](#)].
- [17] A. V. Smirnov and F. S. Chuharev, *FIRE6: Feynman Integral REDuction with Modular Arithmetic*, *Comput. Phys. Commun.* **247** (2020) 106877, [[1901.07808](#)].
- [18] R. N. Lee, *LiteRed 1.4: a powerful tool for reduction of multiloop integrals*, *J. Phys. Conf. Ser.* **523** (2014) 012059, [[1310.1145](#)].
- [19] R. Br user, Z. L. Liu and M. Stahlhofen, *Three-Loop Quark Jet Function*, *Phys. Rev. Lett.* **121** (2018) 072003, [[1804.09722](#)].
- [20] A. von Manteuffel, E. Panzer and R. M. Schabinger, *A quasi-finite basis for multi-loop Feynman integrals*, *JHEP* **02** (2015) 120, [[1411.7392](#)].
- [21] E. Panzer, *Algorithms for the symbolic integration of hyperlogarithms with applications to Feynman integrals*, *Comput. Phys. Commun.* **188** (2015) 148–166, [[1403.3385](#)].
- [22] G. P. Korchemsky and A. V. Radyushkin, *Renormalization of the Wilson Loops Beyond the Leading Order*, *Nucl. Phys. B* **283** (1987) 342–364.
- [23] S. Moch, J. A. M. Vermaseren and A. Vogt, *The three-loop splitting functions in QCD: The non-singlet case*, *Nucl. Phys.* **B688** (2004) 101–134, [[hep-ph/0403192](#)].
- [24] A. H. Hoang, A. Pathak, P. Pietrulewicz and I. W. Stewart, *Hard Matching for Boosted Tops at Two Loops*, *JHEP* **12** (2015) 059, [[1508.04137](#)].
- [25] T. Becher and M. D. Schwartz, *A Precise determination of α_s from LEP thrust data using effective field theory*, *JHEP* **07** (2008) 034, [[0803.0342](#)].
- [26] G. Heinrich, S. P. Jones, M. Kerner, V. Magerya, A. Olsson and J. Schlenk, *Numerical scattering amplitudes with pySecDec*, *Comput. Phys. Commun.* **295** (2024) 108956, [[2305.19768](#)].
- [27] A. V. Smirnov, N. D. Shapurov and L. I. Vysotsky, *FIESTA5: Numerical high-performance Feynman integral evaluation*, *Comput. Phys. Commun.* **277** (2022) 108386, [[2110.11660](#)].